Grain Boundary Segregation in Commercial Nuclear Reactor Pressure Vessel Steels

Grain boundary (GB) segregation of impurity/solute atoms in surveillance test specimens of a commercial western-type pressurized water reactor pressure vessel (RPV) steel has been observed by using state-of-the-art 3D atom probe (3DAP) field ion microscope (laser-assisted local electrode-type atom probe: laser-LEAP). The GB segregation is considered to be an origin of the embrittlement of the RPV steels without hardening. After the low dose irradiation, P, C and Mo atoms are segregated on GB. After the high dose irradiation, the segregation of Si, Mn and As atoms, in addition to P, C and Mo, is observed.

The irradiation-induced embrittlement of the nuclear reactor pressure vessel (RPV) steels is currently a vital issue for ensuring safe operation of nuclear power plants in the world since the reactors of the first generation are going to exceed their initially designed operation lifetimes. Thus, it is of great importance to reveal the nanostructural change, attributed to the origins of the embrittlement, during long-term operation of the commercial nuclear reactors [1,2].

Here we show the grain boundary (GB) segregation of impurity/solute atoms in surveillance test specimens of a RPV steel with high Cu impurity (0.30 wt.%); pressurized water reactor (PWR), Doel-2 (in Belgium), by using laser-assisted local electrode- type 3D atom probe (laser-LEAP). The GB segregation is a possible candidate of the embrittlement of RPV steels without hardening. Since the embrittlement by the GB segregation is considered to be noticeable after high dose irradiation , the detailed observation of the GB is very important for aged RPVs.

The key for the successful observations is to prepare fine needle specimens with GB at few ten nm below the top of the needles. We successfully made the specimens by combining focused ion beam (FIB), electropolishing and transmission electron microscope (TEM). Another key is to use new 3DAP, laser-LEAP. It enables us to analyze much larger volume than conventional 3DAP and to reduce the possibility of the fracture of the irradiated needle specimens.

Figure 1 shows 3DAP atom maps of the solute distributions in Doel-2 RPV surveillance test specimens, around GB, of low dose ((a) 0.83×10^{19} n/cm^2) and high dose ((b) 5.1×10^{19} n/cm^2), corresponding to the in-service irradiation periods for about 3 and 20 years, respectively. After the low dose irradiation, the segregation of P, C and Mo atoms on GB is clearly observed. Precipitation of Cu on the GB is also observed. After the high dose irradiation, Si, Mn and As atoms are segregated in addition to P, C and Mo.

We also observed low angle GB in the high dose specimen. As shown in Fig.2(a), P and C atoms are segregated and Cu atoms are precipitated on the GB. (Mo is also segregated, although it is not plotted in the figure.) However, in this case, the segregation is not uniform on the GB surface. Figure 2(b) shows the lines of P and C atoms in the same spacing. These lines correspond to the array of dislocation lines, and P and C are segregated along the dislocations. The Cu precipitates are also on the dislocation lines [3].
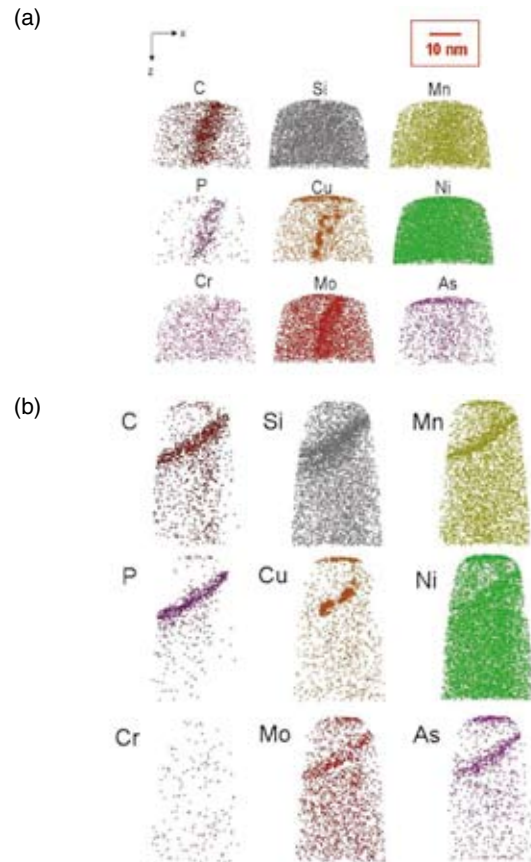

Fig. 1. 3DAP atom maps of RPV surveillance test specimens of Doel-2 with GB. (a) 0.83×10^{19} n/cm^2, (b) 5.1×10^{19} n/cm^2.
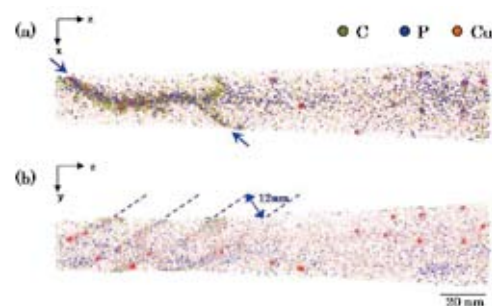

Fig. 2. 3DAP atom maps for low angle GB.

References
[1] Y.Nagai, T.Toyama, Y.Nishiyama, M.Suzuki, Z.Tang and M.Hasegawa, Appl. Phys. Lett. **87**, 261920 (2005).
[2] T.Toyama, Y.Nagai, Z.Tang, M.Hasegawa, A.Al Mazouzi, E.vav Walle, R. Gerard, Acta Materialia **55**, 6852 (2007).
[3] T. Toyama, Y.Nagai and M.Hasegawa, MTERE **46**, 812 (2007) (in Japanese).

Contact to
Yasuyoshi Nagai (Irradiation Effects in Nuclear and Their Related Materials Division)
e-mail: nagai@imr.tohoku.ac.jp

Effects of Electron and Neutron Irradiations on the Properties of Functional Materials for Fusion Applications: Role of Hydrogen in Radiation Effects on Oxide Ceramics

Effects of hydrogen (proton) in the electrical conductivity of ceramics were studied, with protonic conductive perovskite-oxides. Large electrical conductivity was observed at elevated temperatures under fission reactor irradiation, which could be explained by the contribution of protonic conduction. At elevated temperatures, existence of high concentration hydrogen (proton) will increase the ionic conductivity. Reduction of ions constituting the oxides was observed in electron irradiation as well as 14 MeV neutron irradiation at room temperature, which will result in radiation induced phase changes. The results imply that role of hydrogen in radiation effects in oxide ceramics is important, which may evoke technological problems in fusion machines.

The behavior of electrical conductivity of perovskite-oxides was evaluated, under 1.8–2.0 MeV electrons, 14 MeV neutrons and fission reactor irradiations. Effects of hydrogen (protons) on the electrical conductivity were specially studied. All of the perovskite-oxides studied had relatively large base electrical conductivity and normal RIC by the excited electrons was marginal in the irradiation. The electrical conductivity of $SrCe_{0.95}Yb_{0.05}O_{3-\delta}$ increased by 8×10^{-9} S/m from the base electrical conductivity under the 1.8 MeV electron irradiation [1] with a 10 Gy/s dose rate, which is within the range of scatter of accumulated data of the radiation induced electrical conductivity (RIC) of several ceramic insulators shown in Fig. 1. In the meantime, the base electrical conductivity decreased from 4.6×10^{-8} S/m to about 5×10^{-10} S/m after the 2.85 MGy irradiation. A similar decrease of the base electrical conductivity was observed in the 14 MeV neutron irradiations at 293 and 373 K [2]. The observed decrease of the base electrical conductivity is thought to be related to a radiation induced reduction, namely change of a charge state of ions in the oxides. In the case of $SrCe_{0.95}Yb_{0.05}O_{3-\delta}$, Ce^{4+}, this may being reduced to Ce^{3+}.

With decrease of the base electrical conductivity from 2×10^{-8} S/m to about $(2-5) \times 10^{-10}$ S/m, a radiation induced (enhanced) electrical conductivity of about 2×10^{-9} S/m
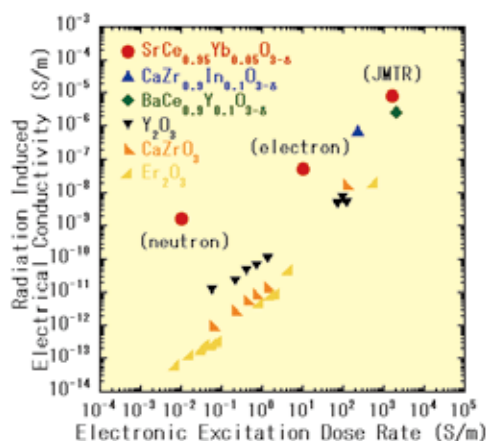

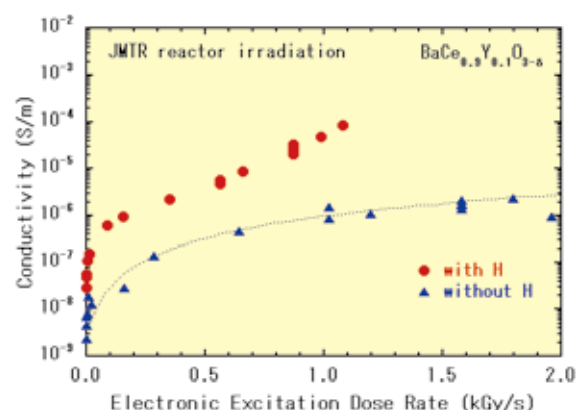Fig. 1. Radiation induced electrical conductivity (RIC) of several ceramic insulators.

Fig. 2. Electrical conductivity of $BaCe_{0.9}Y_{0.1}O_{3-\delta}$ during JMTR startup operation.

surfaced even in 14 MeV neutron irradiation at 293 K [2], after the irradiation up to about 2×10^8 n/m^2. The electronic excitation dose rate was estimated to be in the range of 10^{-2} Gy/s and the observed increase of the electrical conductivity was higher than the accumulated RIC data as shown in Fig. 1. Hydrogen atoms picked up from the atmospheric environment may play a role in the observed radiation induced (enhanced) electrical conductivity.

The electrical conductivities of $BaCe_{0.9}Y_{0.1}O_{3-\delta}$ with one hydrogen implanted in its anode zirconium film and another without hydrogen implantation are shown in Fig. 2 as a function of the electronic excitation dose rate at the startup of JMTR [3]. It is clearly shown that the specimen with hydrogen had larger electrical conductivity than that without hydrogen. Two other oxides, $SrCe_{0.95}Yb_{0.05}O_{3-\delta}$ and $CaZr_{0.9}In_{0.1}O_{3-v\delta}$ showed similar results. The results clearly showed that the hydrogen implantation into an anode increased the electrical conductivity. The observed increase of electrical conductivity, both in the specimens with hydrogen and without hydrogen, with the increase of the reactor power (thus the increase of the neutron flux and the electronic excitation dose rate) does not directly correspond to the increase of the normal RIC. In normal RIC, the electronic conductivity is dominant and the RIC has very weak temperature dependence, in the present case, the electrical conductivity observed during the JMTR irradiation had a large temperature dependence.

References
[1] B. Tsuchiya, A. Moroño, E.R. Hodgson, T. Yamamura, S. Nagata, K. Toh, T. Shikama, Phys. Stat. Sol. (C) **2**, (1), 204 (2005).
[2] B. Tsuchiya, S. Nagata, K. Toh, T. Shikama, M. Yamauchi, T. Nishitani, Fus. Sci. Technol. **47**, (4), 891 (2005).
[3] T. Shikama, B. Tsuchiya, E. R. Hodgson, J. Nucl. Mater. **367-370**, 995 (2007).

Contact to
Tatsuo Shikama (Nuclear Materials Science Division)
e-mail: shikama@imr.tohoku.ac.jp

Effects of Impurities on One-dimensional Migration of Interstitial Clusters in Iron under Electron Irradiation

One-dimensional (1D) migration of small interstitial-type dislocation loops was studied for iron specimens of different purities under electron irradiation using a high-voltage electron microscope. The distance and frequency of 1D jumps were greatly reduced by impurity atoms. We proposed a model describing the experimental 1D jump behavior with a support by molecular dynamics simulations.

Recent molecular dynamics (MD) simulations of displacement collision cascades in copper and iron have suggested that interstitial clusters are directly formed from cascade damage and that the clusters escape from the cascade damage zone through one-dimensional (1D) migration with an activation energy as low as 0.03-0.05 eV. Migration of single vacancies, on the other hand, is through a three-dimensional (3D) random walk. The difference in the migration mechanism between interstitial atoms (including their clusters) and vacancies has been shown to affect total defect structural development under irradiation with high-energy particles. Therefore, the study of 1D migration is important for materials development for future nuclear applications. In addition, recent years have seen a renewal of interest in the nature of self-interstitial atoms and their clusters: the 1D migration observed in experiments and MD simulations raises a question about our understanding of the configuration and migration of this basic unit of crystal lattice defects in both fcc and bcc metals.

We investigated the experimental 1D migration of interstitial clusters in iron specimens of different purities under electron irradiation using a JEMARM-1250 high-voltage electron microscope at Tohoku University. Most 1D migration appeared as discrete jumps (stepwise positional changes) at irregular intervals, and sometimes involved back and forth motion between certain points. The distribution of jump distances extended to over 100 nm in high-purity specimens; it was less than 30 nm in low-purity specimens. Jump frequency was almost proportional to electron beam intensity, and was on the same order as the rate of atomic displacement by electron irradiation.

Molecular dynamics simulation suggested the suppression of 1D migration of an interstitial cluster (7i) by an oversized solute Cu atom located in the dilatational strain field of the cluster. We proposed that the 1D jump process occurs in the following sequence: (1) interstitial clusters in a stationary state being trapped by impurity atoms, (2) detrapping from impurity atoms caused by displacement of impurity atoms by incident electrons, (3) fast 1D
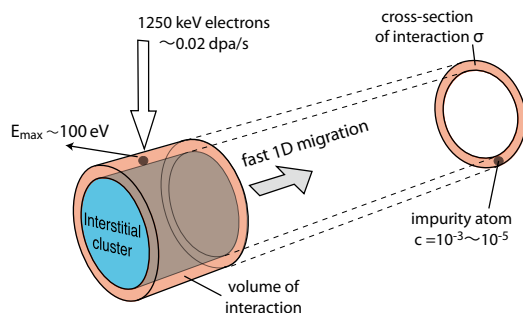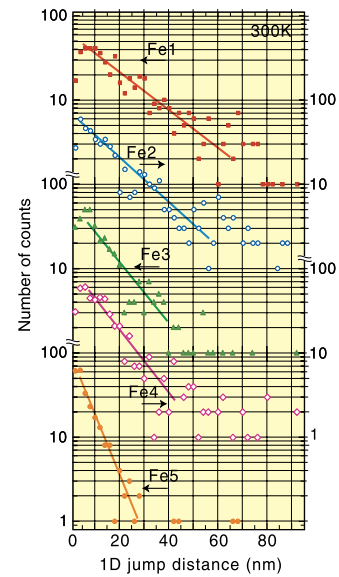
Fig. 2 Distribution of 1D jump distances observed in five iron specimens from high (Fe1) to low (Fe5) purities under irradiation with 1250 kV electrons at room temperature.

migration of liberated clusters at low activation energy, and (4) another trapping by some impurities. Figure 1 schematically shows the present model.

Based on the proposed model, we consider a certain volume around individual interstitial clusters, and assume that a certain impurity atom in this volume prevents the free migration of an interstitial cluster due to their binding. Let the cross-section of the interaction volume projected along the direction of 1D migration be σ. We also assume a random distribution of impurity atoms at the concentration C_i ($<<1$) and neglect the migration of impurity atoms during the fast 1D migration of interstitial clusters for simplicity. Then a 1D jump of length n, namely, an interstitial cluster detrapped from an impurity atom and trapped again by another impurity atom after 1D migration for n atomic distances, is approximated to have a probability of $P(n) = (1-\sigma C_i)^{n-1} \cdot \sigma C_i$.

The distribution of 1D jump distance in iron specimens from high (Fe1) to low (Fe5) purities is plotted in Fig. 2. When we neglect the region of jump distances less than 10 nm for experimental difficulties and also that of long distances for poor statistics, the middle range for each specimen is well described by the straight line. The σC_i values obtained from the gradient of the line were greater for the low-purity specimens, and corresponded to the results of chemical impurity analysis of the specimens. The experimental 1D migration behavior was successfully explained by the simple model.

Reference

[1] Y. Satoh, H. Matsui, T. Hamaoka, Phys. Rev., B**77**, 94135 (2008).

Contact to
Yuhki Satoh (Nuclear Materials Engineering Division)
e-mail: ysatoh@imr.tohoku.ac.jp

Fig. 1 Schematic illustration of the present model of 1D jumps of interstitial clusters observed under HVEM irradiation conditions.

Development of Ultra-fine Grained W-(0.25-0.8)wt%TiC and Its Superior Resistance to Neutron and 3MeV He-ion Irradiations

Poor ductility and radiation induced embrittlement due mainly to weak grain boundaries in tungsten have been major concern with its application. This summary document describes the current status on the developmental work performed to mitigate the issue [1].

Tungsten (W), a refractory transition metal in group VIA, is the most promising for use as divertors and structural materials exposed to high heat loading and irradiation environments because of its high melting point, good thermal conductivity, low thermal expansion coefficients, reduced radio activation, etc. However, it undergoes serious embrittlement in several regimes, i.e., low temperature embrittlement, recrystallization embrittlement and radiation embrittlement.

For the mitigation of the issue, we have developed ultra-fine grained (UFG) W-TiC with average grain sizes of 50 ~ 200 nm and a relative density of approximately 99% by utilizing mechanical alloying (MA) and hot isostatic pressing (HIP) processes. Such UFG W-TiC consolidates exhibited a maximum fracture strength of approximately 2GPa at room temperature,however no ductility is assured prior to fracture. The assurance of room-temperature ductility hence remains to be accomplished for UFG W-TiC.

A noted finding regarding this respect is that plastic working after consolidation significantly increases the fracture strength accompanied with appreciable room-temperature ductility and the ductility increase becomes prominent with decreasing grain size from 2 to 0.6μm [2]. Therefore, the above main problem is expected to be overcome by applying a sufficient degree of plastic working without a significant change in the UFG structures (grain size: 0.05-0.2μm) to poorly workable W-TiC. UFG materials are known to exhibit superplasticity. Superplastic deformation can be utilized as a plastic working process for poorly workable W-TiC and thus it is important to reveal high temperature deformation of UFG W-TiC in connection with superplasticity.

Regarding radiation resistance of W-TiC, on the other hand, it has been shown that fine-grained W-0.3TiC (grain size: 0.9μm) exhibits higher resistance to neutron irradiation at 563K to 9×10^{23} n/m^2 ($\underline{E}$ > 1MeV) than commercially available pure W [3]. However there are no reports on the effects of neutron and He ion irradiations for UFG W-TiC.

The objective of this study is to show the features of microstructures and mechanical properties at room and high temperatures in the unirradiated state. Effects of irradiation with neutrons or 3MeV helium-ions on microstructures and room temperature mechanical properties are also presented.

Neutron irradiation was performed in a helium atmosphere to a fluence of 2×10^{24} n/m^2 (about 0.15 dpa) at 873K in the Japan Materials Testing Reactor (JMTR). For comparison, TEM disks of commercially available pure W with a grain size of approximately 10μm in the hot-rolled, stress-relieved condition were also prepared and examined.

He irradiation was conducted for the TEM disk specimens by a dynamitron type accelerator at Tohoku University with 3 MeV He^{4+} at 823 K up to a fluence of 10^{23} He/m^2.

The main results and conclusions are as follows [1]:

1. The microstructural features of UFG W-(0.25-0.8)%TiC are equiaxed grains with average diameters of 50 to 190nm and nearly full density of approximately 99%. Significant grain refinement occurs by TiC additions and use of Ar in the MA atmosphere which gives rise to a large number of nano-size Ar bubbles in the as-HIPed W-TiC consolidates.

2. Vickers microhardness (HV) values of UFG W-TiC are in a range of 900 to 1160 and determined by grain size strengthening.

3. The three-point bend fracture strength at room temperature depends strongly on the TiC addition and MA atmosphere. The strength takes a maximum of approximately 2GPa for 0.25~0.5%TiC additions and increases in the order of H_2, Ar and N_2 as the MA atmosphere, which is mainly attributable to decrease in detrimental effects of pores and/or bubbles due to easier removal of H_2 than Ar and N_2 from the W-TiC consolidates.

4. W-0.5TiC/H_2 exhibits superplastic deformation at 1673-1973K, with a larger strain rate sensitivity of flow stress, *m*, of 0.5~0.6. On the other hand, W-0.5TiC/Ar does not exhibit superplastic deformation, with a smaller m value of approximately 0.2 [4]. This suggests that the Ar bubbles cause an adverse effect on superplastic deformation.

5. For fast neutron irradiation to a fluence of 2×10^{24} n/m^2 at 873K, W-0.5TiC/H_2 and W-0.5TiC/Ar exhibit no radiation hardening as measured with Vickres microhardness, whereas commercially available pure W shows a considerable hardening of ΔHV = 98. Radiation induced interstitial loops and voids are observed with much less increase in void density for UFG W-0.5TiC than that for commercially available pure W. No significant difference in radiation hardening between the consolidates fabricated via the different MA atmospheres is recognized under this irradiation condition.

6. The critical fluence for exfoliation and surface cracking along grain boundaries to occur by 3MeV He irradiation is about 2×10^{22} He/m^2 for commercially available W materials (pure W/R, K-doped W/R and K-doped W/SR. R: Recrystallized, SR: Stress Relieved) and above $2\sim3\times10^{23}$ He/m^2 for UFG W-0.3TiC/H_2. This indicates that surface damage resistance to 3 MeV He irradiations for UFG W-0.3TiC/H_2 is more than ten times as high as that for the commercially available W materials.

References

[1] H. Kurishita, S. Kobayashi, K. Nakai, T. Ogawa, A. Hasegawa, K. Abe, H. Arakawa, S. Matsuo, T. Takida, K. Takebe, M. Kawai and N. Yoshida, J. Nucl. Mater. **377**, 34 (2008).

[2] Y. Ishijima, H. Kurishita, H. Arakawa, M. Hasegawa, Y. Hiraoka, T. Takida and K. Takebe, Mater. Trans. **46**, 568(2005).

[3] H. Kurishita, H. Arakawa, Y. Amano, S. Kobayashi, K. Nakai, H. Matsui, Y. Hiraoka, T. Takida and K. Takebe, J. Nucl. Mater. **367-370**, 1453 (2007).

[4] H. Kurishita, S. Matsuo, H. Arakawa, S. Kobayashi, K. Nakai, T. Takida, K. Takebe and M. Kawai, Mater. Sci. Eng. A**477**, 162 (2008).

Contact to

Hiroaki Kurishita (International Research Center for Nuclear Materials Science)

e-mail: kurishi@imr.tohoku.ac.jp